2D inverse modeling of sedimentary basin subsidence

Poplavskii, K.N.; Podladchikov, Y.Y.; Stephenson, R.A.

published in
Journal of Geophysical Research. Solid Earth
2001

DOI (link to publisher)
10.1029/1999JB900211

document version
Publisher's PDF, also known as Version of record

JOURNAL OF GEOPHYSICAL RESEARCH, VOL. 106, NO. B4, PAGES 6657–6671, APRIL 10, 2001

Two-dimensional inverse modeling of sedimentary basin subsidence

Konstantin N. Poplavskii[1]

Institute of Geophysics, National Academy of Sciences of Ukraine, Kiev, Ukraine

Yuri Y. Podladchikov

Geologisches Institut, ETH-Zurich, Zurich, Switzerland

Randell A. Stephenson

Department of Sedimentary Geology, Vrije Universiteit, Amsterdam

Abstract. Recently developed mathematical models of subsidence in extensional basins provide a good basis for forward modeling. However, the large number of parameters to be specified by the user makes it difficult not only to do the modeling itself, but also to judge the meaning of the results. We present a new method for automatic searching of the best-fitting parameter set of a 2D basin formation model. Weighted goal functions are used in the minimization process by the inverse problem solver algorithm. The nominal parameter set in the present case includes profiles of the crustal and subcrustal thinning factors, and the level of lithosphere necking. The method was tested on synthetic data with parameters that were perturbed beforehand. With some restrictions, the algorithms are capable of resolving such perturbations. The inversion technique has been applied to two profiles crossing the Dnieper-Donets Basin (Ukraine). The crustal thinning factors obtained argue for a scissors-like style of basin opening. High subcrustal thinning values are necessary in order to explain the abnormally thick Carboniferous section in the basin. These values should be treated as cumulative ones due to the currently unresolvable influence of other rifting-related processes, particularly phase transitions.

1. Introduction

Recently developed mathematical models of rifted sedimentary basin evolution that elaborate on the basic lithosphere stretching model of *McKenzie* [1978] incorporate the rheological, thermal, and flexural isostatic consequences of lithosphere extension, providing good facilities for two-dimensional forward modeling [e.g., *Stephenson et al.*, 1989; *Cloetingh and Kooi*, 1992; *Kusznir and Ziegler*, 1992; *Starostenko et al.*, 1996]. Pioneer works of *White* [1993, 1994] present the first method for inversion of the stratigraphic record. Albeit in one dimension, the method results in numerical estimates of the lithospheric strain rate and its evolution in time, explaining all basic features of the observed subsidence curves. This inversion method is based, however, on the uniform stretching model, which limits its applicability for our modeling goals. Most of the contemporary two-dimensional (2-D) forward modeling techniques have a large number of parameters that must be specified by the user. This makes it difficult to interpret the results in terms of the sensitivities or dominance of the various parameters. The most laborious part is the search of the optimal set of thinning factors. The inverse modeling procedure presented here has been developed in order to provide an automatic search of the best fit parameter set. Additionally, the inverse modeling can assure that the data have been fit to minimize a particular norm. An easy access to the formal best fit allows many more numerical experiments while modeling and leads eventually to a better understanding of the processes being modeled.

The inverse modeling procedure includes a forward problem solver. The input data for the forward problem solver consist of a particular set of parameters which describe the state of the lithosphere prior to rifting and the thermomechanical effects of a given lithosphere-rifting process. The output data represent the resulting basin stratigraphy at any time thereafter. From the final basin shape, the gravity anomalies and Moho geometry can be readily obtained. The inverse modeling procedure manages the parameters in order to improve the fit between the observed and calculated stratigraphy. The estimate of the misfit between these is referred to as the "goal function" and is the function for which a minimum is to be found. The misfit between the observed and calculated present-day thicknesses of the stratigraphic layers of a sedimentary basin is an obvious candidate for the role of the goal function. Generally, this misfit value (the "global" misfit) should include the differences between every observed and calculated value. In the present case, it means the differences between observed and calculated stratigraphic thicknesses for each horizon for a chosen number of points on a cross-section. In such a case, the minimization procedure will be equally sensitive for all data

[1]Now at Geosciences Department, University of Houston, Houston, Texas.

Paper number 1999JB900211.
0148-0227/01/1999JB900211$09.00

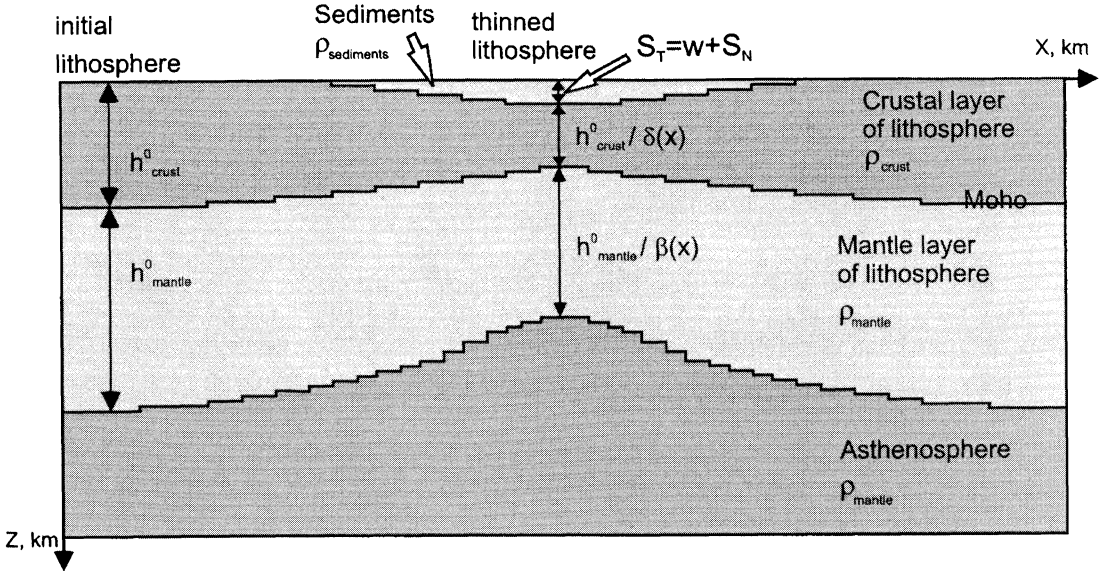

Figure 1. Formulation of the problem. $S_T(t,...)$, time-dependent total basin subsidence; $w(x,...)$, flexural deflection of the thin elastic plate; $S_N(x, \delta, Z_{neck},...)\,|_{t=0}$, necking-induced geometry at the end of the rifting; $\delta(x)$, thinning factor (crustal lithosphere layer); $\beta(x)$, thinning factor (subcrustal lithosphere layer); h^0_{crust}, thickness of the initial crustal lithosphere layer; h^0_{mantle}, thickness of the initial mantle lithosphere layer; Z_{neck}, depth of necking level as chosen for modeling; ρ_{crust}, density of the crustal lithosphere layer; ρ_{mantle}, density of the mantle lithosphere layer; X, horizontal coordinate; Z, vertical coordinate; t, time.

observed. However, the parameters inherent to the forward modeling procedure can contribute to the calculated stratigraphy in rather different ways.

In general, the inverse modeling consists of finding the minimum of the chosen goal function. An essential factor is the appropriate choice of the goal function and of the minimization method for different model parameters. Additionally, a priori information should be used to define ranges of values for these parameters. This includes general geological information, for example, such predefined parameters as compaction coefficients, rock densities for crust and mantle, etc. Other kinds of geological and geophysical data sets, specific for the particular basin being studied, should be used to constrain initial crust and lithosphere thickness as well as time and duration of rifting events.

Thus we define the objective of the inverse modeling process as finding the set of particular parameter values, restricted by a priori known limits, which result in a satisfactory fit of model predictions to the observed basin stratigraphy. This is rather similar to the practical work of most basin modelers.

2. Method

2.1. Formulation of the problem

2.1.1. Forward problem solver. We consider the process of basin formation as a procedure ("forward problem solver" or "operator F") which, being applied to some part of the lithosphere, deterministically gives a certain basin stratigraphy. The forward problem solver used in the present case is that of *Kooi et al.* [1992] and *Kooi and Cloetingh* [1992], which is a model based on the lithosphere stretching assumptions originally formulated by *McKenzie* [1978] but extended to include the possibility of a finite duration of rifting [e.g., *Jarvis and McKenzie*, 1980], nonhomogeneous thinning of the crustal and subcrustal parts of the lithosphere [e.g., *Royden and Keen*, 1980], the effects of in-plane stresses on flexure [e.g., *Stephenson and Lambeck*, 1985; *Cloetingh et al.*, 1985; *Karner*, 1986], and the isostatic effects of a strong lithosphere layer controlling a necking depth during rifting [e.g., *Braun and Beaumont*, 1989].

In accordance with the methodology developed by *Kooi et al.* [1992], it is assumed that the thinned part of the lithosphere can be approximated in two dimensions by a set of vertical blocks, called boxes, of equal width. Each block is characterized by a crustal (δ) and subcrustal (β) lithosphere thinning factor. The thinning factor is defined as a ratio of the thickness of the lithospheric layer at a given point after stretching to the thickness of unstretched layer.

Depth of necking Z_{neck} is defined as the level of zero vertical displacement of lithosphere, in the absence of gravity, during rifting [*Kooi and Cloetingh*, 1992]. The depth of necking Z_{neck} strongly influences the kinematic subsidence S_{neck}, which is the subsidence of the surface of the thinned lithosphere in the absence of the isostatic compensation. S_{neck} depends on thinning factors, lithosphere geometry, and lithosphere material properties (ρ_{mantle} and ρ_{crust}, h^0_{crust} and h^0_{mantle}, etc.; see Figure 1). The minimum value of Z_{neck} is zero, which provides a model equivalent to McKenzie's [*Kooi and Cloetingh*, 1992]. The maximum possible value is $h^0_{crust}+h^0_{mantle}$.

We consider also the effects of in-plane stresses N_k, operating during each kth geological stage presented in the observed postrift stratigraphy, as defined in the thin elastic plate flexure equation as follows [after *Kooi and Cloetingh*, 1992]:

$$\frac{\partial^2}{\partial x^2}\left[D(x)\frac{\partial^2 w(x)}{\partial x^2}\right]+N_k\frac{\partial^2 w(x)}{\partial x^2}+(\rho_m-\rho_s)gw(x)=q(x) \qquad (1)$$

Table 1. Parameters and Notations Used in Equations

Notation	Meaning	Value
H_m	mantle lithosphere thickness	135 km
N_b	number of boxes in the optimized part of model	50
H_f	sedimentary layer thickness	Variable
ρ_f	sedimentary layer density	Variable
τ	thermal relaxation constant	62.8 Ma
$W(x)$	flexural response of the lithosphere	Variable
$D(x)$	flexural rigidity of the lithosphere	Variable
N	Horizontal loads on the lithosphere	Variable
ν	Poisson's ratio	0.25
E	Young's modulus	7×10^{10} Pa
T	temperature	Variable
T	Time	Variable
X	Horizontal coordinate	Variable
Z	vertical coordinate	Variable

Parameters and notations not explained immediately after first appearance are given in Table 1. See also Table 2 for the full set of the forward problem solver parameters.

Following *Kooi et al.* [1992], flexural rigidity D is determined in terms of an effective elastic thickness (EET) defined by the depth to a given isotherm. Hence EET is a constant neither in space (along the cross section) nor in time. The final subsidence S_{total}, calculated by the forward problem solver F, is the sum of the various displacements S_{neck}, $w(x)$, and terms related to the thermal loading of the lithosphere.

It is not intended here to invert the forward modeling procedure analytically; the reader is therefore referred to *Kooi et al.* [1992, and references therein] for further details of the present "forward problem solver" algorithm.

2.1.2. Formulation of the inverse problem. Lithosphere material properties X^{prop} and lithosphere rifting process parameters X^{proc}, which ultimately define the result, are combined in a set of input parameters X which must be completely predefined for the forward problem solver. Sometimes, the set of input parameters X will be referred to as vector X, a point in the linear vector space P (parameter space [cf. *Menke*, 1984]) having N_p dimensions.

The forward problem solver output consists of the calculated basin stratigraphy and is called vector Y. Vector Y may be represented by the point in the linear vector space M (model state space) having N_o dimensions. N_p is equivalent to the number of model parameters, and N_o is equivalent to the number of observations. Note that in the general case, $N_o \geq N_p$. In a similar manner, observed stratigraphy is $Y_{observed}$. Thus the operator F represents the procedure of "mapping" the parameter set X (the point in the parameter space P) to the basin stratigraphy Y (the point in the model state space M).

$$Y = F(X) \tag{2}$$

Table 2. Notations and Values of the Forward Problem Solver Parameter Set

Notation	Meaning	Value		
		Synthetic	Real Models	
		Model	LK	SL
$\delta(x)$	crustal lithosphere thinning factor	max. 1.98	max. 1.8	max. 1.8
$\beta(x)$	mantle lithosphere thinning factor	max. 2.5	max. 5.0	max. 7.0
$t^{rifting}$	beginning of rifting	386 Ma	386 Ma	386 Ma
t_R	rifting duration	36 Ma	36 Ma	36 Ma
t_k	ages of the stratigraphic horizons	see text	see Figure 8	see Figure 9
T_{EET}	isotherm defining EET	220° C	220° C	220° C
Z_{neck}	depth of necking level	10 km	10 km	17 km
N_k	In-plane stresses operating in k th time	see text	see text	see text
N_b	number of boxes in the model	200	200	200
Δx	box width	2 km	2.5 km	2.5 km
T_a	asthenosphere boundary	1333° C	1333° C	1333° C
h_c	crustal lithosphere thickness	40 km	40 km	40 km
h_L	lithosphere thickness	175 km	175 km	175 km
ρ_c	crustal lithosphere density	2.80 g/sm^3	2.80 g/sm^3	2.80 g/sm^3
ρ_m	mantle lithosphere density	3.33 g/sm^3	3.33 g/sm^3	3.33 g/sm^3
α	thermal expansion coefficient	3.4×10^{-5}° C^{-1}	3.4×10^{-5}° C^{-1}	3.4×10^{-5}° C^{-1}
κ	thermal diffusivity	0.78×10^{-7} m^2/C	0.78×10^{-7} m^2/C	0.78×10^{-7} m^2/C
ρ_s	grain density of the sediments	2.70 g/sm^3	2.70 g/sm^3	2.70 g/sm^3
ϕ_0	porosity of the sediments at the surface	0.55	0.55	0.55
d^C	characteristic depth constant for the porosity-depth relation	0.55 km^{-1}	0.55 km^{-1}	0.55 km^{-1}

Assuming $G(X) = F(X) - Y_{observed}$, the equation to be solved by the inverse problem solver can be written as follows:

$$G(X) = 0. \quad (3)$$

If $Y_{observed}$ and Y both are points in model state space, one can define the distance $d^G{}_i$ (where i is an iteration number) between these two points as an L_2 norm of difference between vectors $Y_{observed}$ and Y, respectively:

$$d^G = \|Y - Y_{observed}\| = \sum_{j=1}^{N_0} \left(Y_j^2 - Y_{observed,j}^2\right) \quad (4)$$

The distance $d^G{}_i$ between the current solution Y_i and the observed data $Y_{observed}$ is treated as a global misfit value and is used as the main goal function to be minimized.

It should be clearly understood that the solution found by the goal function minimization is not necessarily the global one [cf. *Kooi et al.*, 1992; *Watts and Stewart*, 1998]. A full discussion of the existence, uniqueness, and stability of the solution of (3) would require an analytical investigation of the operator F and goes beyond the limits of this paper.

To recapitulate, the parameters of particular interest for our purposes in modeling a 2-D geological cross section will be (1) the crustal thinning factor δ profile; (2) the subcrustal lithosphere thinning factor β profile; and (3) the level of necking Z_{neck}. Note that even with this truncated parameter set, the parameter space still has $2N_b+1$ dimensions, where N_b is the number of boxes in model. For our synthetic model having 50 boxes, the parameter space will have 101 dimensions. The model was padded by 75 boxes from both sides with parameters of the unstretched lithosphere. Other parameters, which are in use by the forward problem solver, are assumed to have fixed values.

Hence we seek a parameter set X_i:

$$X_i = [\,\delta(x), \beta(x), Z_{neck}, \ldots] \quad X_i \in X^R, \quad (5)$$

which gives $Y_i = F(X_i)$ such that $\|Y_i - Y_{observed}\| < \varepsilon$ and $\|Y_i - Y_{i-1}\| > \phi$. X^R stands for the admissible subset of parameters in the parameter space; X_i is an unknown parameter set $[\delta(x), \beta(x), Z_{neck}, \ldots]$; and ε and ϕ are the small numbers defining the precision required during an iterative procedure and the convergence rate, respectively. The subset X^R is assumed to be a continuous domain. It should be outlined in the parameter space X using the a priori defined upper and lower limits for every parameter in use.

2.2. Synthetic and Real Models

In order to promote the construction of the method, a synthetic model was generated, using the same forward modeling code. Disturbances introduced into the synthetic model included arbitrarily determined δ and β factors along the geological cross section and changes of the level of lithosphere necking. In addition, two models based on real data were used. These models are referred to as "real model LK" (profile Losinovka-Kinashevka) and "real model SL" (profile Sagajdak-Lebedin, see section 3 for details). The synthetic model has both a geometry and a parameter set similar to the real geological profiles (see Table 2).

2.3. Initial Guess

The initial guess is a necessary element of the iterative minimization procedure and provides a starting point for the algorithms. Initial values of parameters sought in the inversion process are derived from the simplest model of extensional basin subsidence, assuming local isostasy and uniform instantaneous lithosphere thinning, namely, that of *McKenzie* [1978]. Thus the profile of initial thinning factors $\delta^0(x) = \beta^0(x)$ is calculated in consideration of the local isostatic balance for each box (each x value) on the basis of present-day observed structure and the adopted lithosphere material properties; the depth of necking is zero [*Kooi and Cloetingh*, 1992].

2.4. Preliminary Investigation of the Goal Function Relief

In the formulation of the inverse problem, our task is the minimization of the misfit function. In general, the strategy of the minimization strongly depends on the relief of the goal function. In the case of smooth, single-extremal functions, adaptive algorithms may be used for effective minimization. On the other hand, multiextremal functions in the general case could be minimized either by regular sampling or by some of the Monte Carlo methods only. Note that direct investigation of the relief of a function having about 100 arguments is a rather difficult task. Relief, however, can be analyzed indirectly by applying some widespread optimization algorithms.

A Newton-optimization algorithm was built for simultaneous multiparametric minimization of $d^G{}_i$ goal function. We are considering here a full set of synthetic model parameters. The algorithm delivered rapid convergence to the neighborhood of the minimum of the global misfit, but thereafter the nonlinearity of the problem began to play an increasingly significant role and iterations diverged. The basic features of the algorithm's behavior did not change by truncating the parameter set or through the implementation of various penalty functions. The results of numerical experiments can be summarized as follows. In general, the global misfit function $d^G{}_i$ has a very complicated relief in model state space. In such a case, the adaptive algorithms of multiparametric minimization, based on strong assumptions of goal function smoothness, are either divergent or become "trapped" in a local minimum. Additional problems arise owing to the well-known instability of the inverse modeling of basin thermal history.

Hence we are dealing with a multiextremal function with complicated relief. The regular sampling method is not applicable here owing to unacceptable calculation time. Of course, some of the stochastic optimization techniques such as genetic algorithms could be used. However, their effectiveness strongly depends on fine parameter tuning and usually requires a special analytical investigation. Hence it is expedient to come back to a truncated parameter set and to define different goal functions, specific for each parameter.

2.5. Selection and Minimization of Goal Functions

The general approach taken to the definition of goal functions was (1) to discover which parameters were the most influential (i.e., "first-order"), (2) to find a stable algorithm for their restoration, and (3) to apply the algorithm to determine these first-order parameters. We therefore effectively eliminate

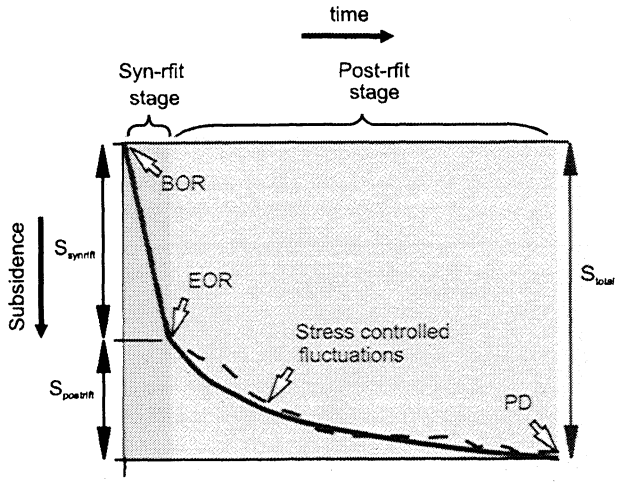

Figure 2. Schematic subsidence curve. Key parameters and their control of basin stratigraphy. BOR, beginning of rifting; EOR, end of rifting; PD, present day; S_{total}, total subsidence; S_{postrift}, thermal postrift subsidence. The post-rift subsidence fluctuations for each age around the "normal" thermal subsidence curve are controlled by intraplate stress operating on that age.

their influence in order to start searching for the optimal value of the next ("second-order") parameter. Otherwise, the model sensitivity to changes in the latter would be masked by the discrepancies between Y_i and Y_{observed} arising from errors in the estimation of the first-order parameters.

In order to find first-order parameters, let us consider the schematic basin subsidence history plotted in Figure 2. The curve is divided into two parts: the synrift phase from the "beginning of rifting" (BOR) to the "end of rifting" (EOR) and the postrift phase from EOR to "present day" (PD). We assume that crustal thinning δ is the main parameter responsible for the total subsidence and that subcrustal thinning β is the most influential parameter for the positioning of the EOR point on the subsidence curve (i.e., in determining the ratio between synrift and postrift subsidence). Intraplate stress variations in time, represented by the second term in (1), will cause minor fluctuations of the postrift subsidence rate around the "normal" thermal subsidence curve defined by δ and β. Numerical experiments (K.N. Poplavskii et al., 2D inverse modeling of intracratonic rift basins: Evaluation of intraplate stresses, submitted to *Tectonophysics*, 1997) (hereinafter referred to as Poplavskii et al., submitted manuscript, 1997) showed that the influence of the in-plane stresses on the subsidence history has much lower magnitude (within the reasonable range of stresses value) than thinning factors variations or changes in level of necking depth.

Thus we assume the δ and β profiles as first-order parameters. The in-plane stresses appear to be a second-order parameter. Albeit the numerical estimate of the distribution of lateral stresses in time could provide us with valuable palaeotectonics information, it is not considered in this study, and the interested reader is referred to Poplavskii et al., (submitted manuscript, 1997). Influence of the necking depth variations cannot be defined directly on the subsidence curve and will be discussed later.

2.5.1. Optimizing of the thinning factors. According to the subsidence curve plotted on Figure 2, we assume the norm $d_i{}^{\delta}$ of the misfit $R_j{}^{\text{total}}$ between total observed and predicted subsidence in each box as a goal function for the searching of δ values. The current total subsidence misfit is defined on ith iteration as

$$d_i{}^{\delta} = \left\| R_i^{\text{total}} \right\| = \left\| S_i^{\text{total}} - S_{\text{observed}}^{\text{total}} \right\| \tag{6}$$

That means that we are seeking $\delta(x)$ that delivers the best fit of the calculated and observed crystalline basement depth along the cross section. This will fix the PD-point on the subsidence curve (Figure 2).

Point EOR on the subsidence curve may be moved only along the vertical axis, changing the amount of postrift subsidence, inasmuch as its horizontal position is fixed by the user-predefined duration of rifting parameter t_R. Hence we choose the norm $d_i{}^{\beta}$ of the misfit $R_i{}^{\text{postrift}}$ between the calculated $S_i{}^{\text{postrift}}$ and observed $S_{\text{observed}}^{\text{postrift}}$ postrift subsidence in each box as a goal function to be minimized while searching for the optimal β values:

$$d_i{}^{\beta} = \left\| R_i^{\text{postrift}} \right\| = \left\| S_i^{\text{postrift}} - S_{\text{observed}}^{\text{postrift}} \right\|. \tag{7}$$

We now have the initial guess and the goal functions for both δ and β, so we may build the iterative procedure $I(X, Y_{\text{observed}})$ for optimizing of the first-order parameters. The Newton optimization method was used to develop an iterative process (optimizing operator I) defined as follows:

$$X_{i+1} = X_i - [G'(X_i)]^{-1} G(X_i). \tag{8}$$

Partial derivatives of δ and β are used here with some modifications. Not every δ_j and β_j value is treated as an independent variable for each jth box. Instead, on each iteration we fix all β values and increment all δ values by the same increment $\Delta\delta$. This results in a partial linearization because the steps for the next iteration are calculated for each jth box separately as if they were actually independent variables. Application of the iterative "optimizing operator" I to parameter set X will give us parameter set X^I. This parameter set has δ and β profiles optimized in the sense of misfit between the modeled and observed stratigraphy Y_i and Y_{observed}, while other parameters remain unchanged.

2.5.1.1. Delta and beta profiles calculation: The partial derivative used for the δ goal function minimization is as follows:

$$R_{i,j}^{\text{total}}{}' = \frac{1}{\Delta\delta}\left[S_j^{\text{total}}(F(\delta_i)) - S_j^{\text{total}}(F(\delta_i + \Delta\delta)) \right], \tag{9}$$

where $S_j{}^{\text{total}}(F(\delta_i))$ is simply an operator extracting the total subsidence value for the jth box. The partial derivative for the β goal function is calculated in a similar manner. The obtained partial derivatives and the $\Delta\delta$ and $\Delta\beta$ increments are then used as usual to update the $\delta_{i,j}$ and $\beta_{i,j}$ values themselves prior to the next iteration.

Such an algorithm results in a rapid and stable convergence not only with respect to the δ and β goal functions but with respect to the global misfit value as well. The convergence is illustrated by Figure 3 in which the δ and β goal functions, the global misfit value, and the integral deviation of the β factor from the δ factor are plotted. The integral deviation of the β factor from the δ factor is defined as follows:

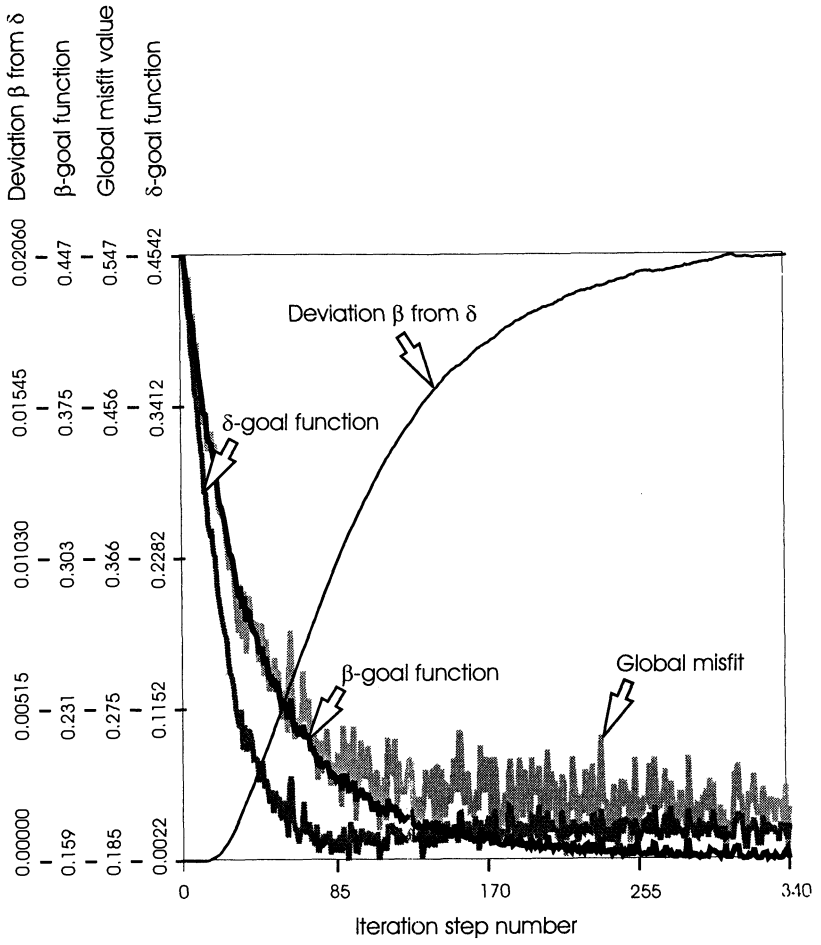

Figure 3. Convergence curves for δ and β factors restoring by "optimizing operator" I (synthetic model). Iteration step length is artificially decreased 100 times for demonstration purposes. Note that deviation of β factor from δ factor starts from 0 with initial guess model and asymptotically reaches a constant value.

$$d^{\beta\delta} = \int \left\| \delta(x) - \beta(x) \right\| \partial x \approx \frac{1}{N_b} \sum_{j=1}^{N_b} \left\| \delta_j - \beta_j \right\|. \qquad (10)$$

2.5.1.2. Thermal filtering procedure for beta profile: The implementation of the operator I described above gives the δ factor profile restored within the given precision range, but the solution is not unique, at least with respect to the β factor. Because of the properties of the heat conduction equation used in the forward problem solver, the calculated final stratigraphy Y is insensitive to the β factor relief along the basin but for its integral value only. This was verified by numerical experiments and is clearly demonstrated in plots of the optimized δ and β profiles (Figure 4). Therefore, in order to restrict the nonuniqueness of the solution, it is necessary to apply some additional requirements for the β factor profile.

Consider the following regularization (filtering) procedure. Let $B(\beta)$ be a function converting $\beta(x)$ into initial temperature distribution $\overline{T}^{\text{inst}}$ assuming instantaneous subcrustal lithosphere stretching:

$$\overline{T}^{\text{inst}} = B(\beta), \qquad (11)$$

where the bar implies the z average: $\overline{T} = \int T \partial z$.

Assume that the synrift evolution of temperature distribution $\overline{T}(x,t)$ can be approximately described by the simple 1-D diffusion equation:

$$\frac{\partial T}{\partial t} = \kappa \frac{\partial^2 T}{\partial x^2}. \qquad (12)$$

Note that only lateral "heat" variations are taken into account. Then let us introduce the "cooling operator" Q, converting temperature distribution $T^{(0)}|_{t=0}$ to the temperature distribution $T^{(1)}|_t$:

$$\overline{T}^{(1)} = Q\left(\overline{T}^{(0)}, t\right), \qquad (13)$$

where $T^{(0)}$ has meaning of the temperature distribution in the stretched lithosphere at the time of the beginning of rifting and $T^{(1)}$ is the temperature distribution at the end of rifting event. Let the "thermal filtering operator" Φ be

$$\beta = \Phi\left(\beta^0, t_f\right), \qquad (14)$$

where β^0 is the unmodified β factor profile as it was initially suggested by the operator I and t_f is the "duration" of the "cooling" (the "duration" of the thermal filtering operation), such that Φ operates in a similar manner to (12):

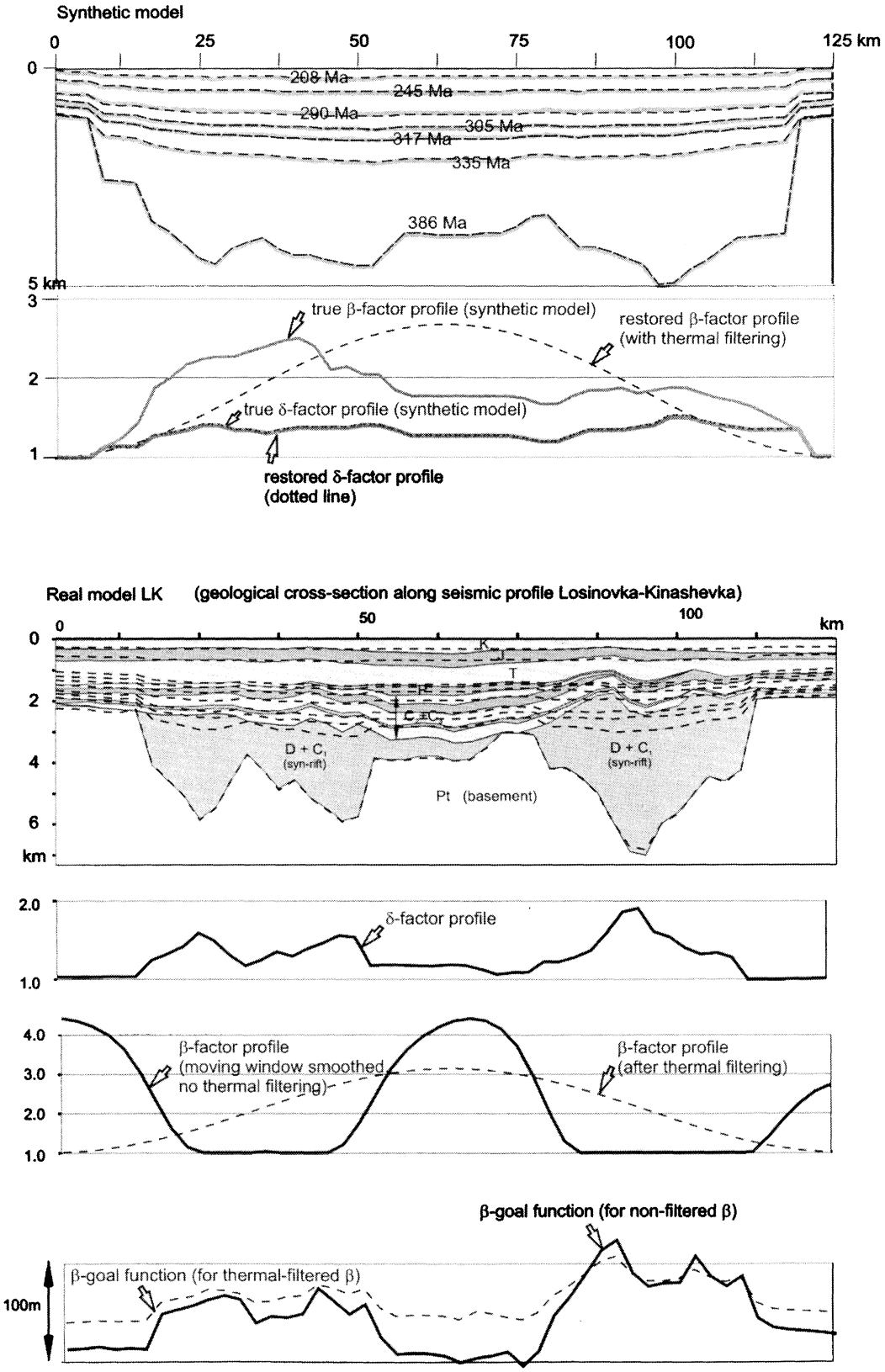

Figure 4. Stratigraphy of the synthetic model and "true" and restored thinning factor profiles. Sketch of stratigraphy of the real model LK (profile Losinovka-Kinashevka) with optimized δ and β factors profiles. β factor profiles and β goal function plots for both thermal filter processed and nonfiltered β.

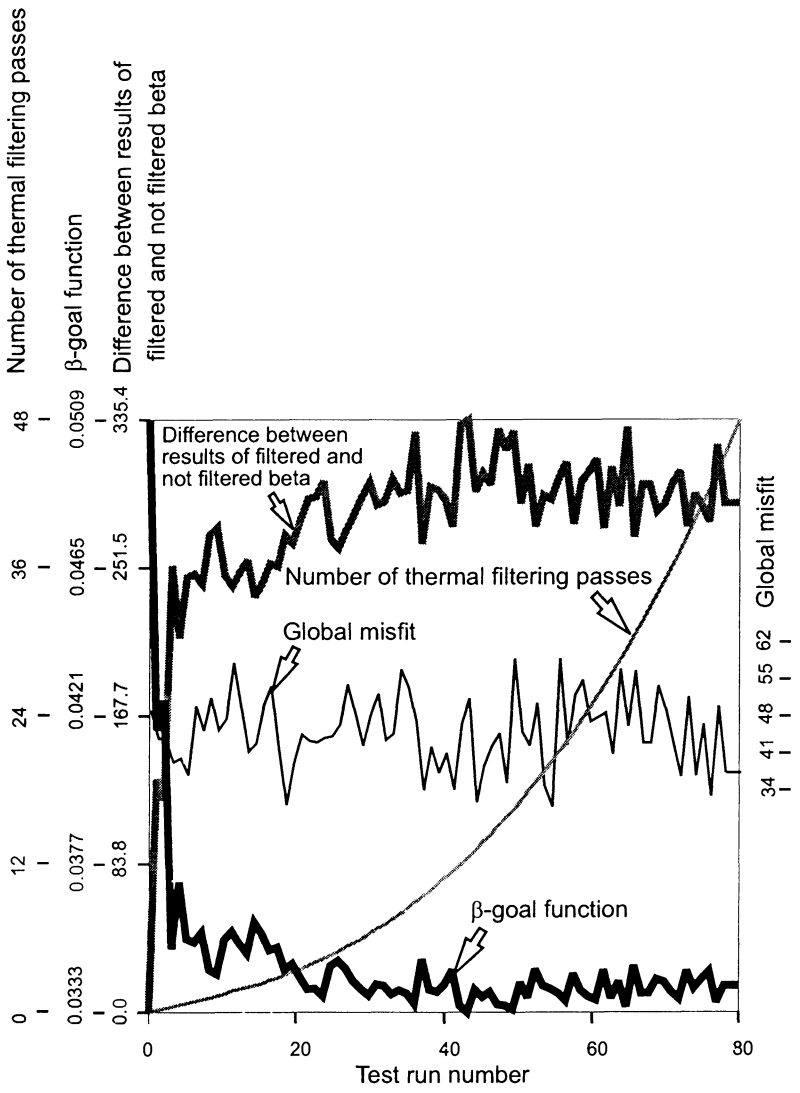

Figure 5. Curves illustrating results of thermal filtering of β factor profile. Note that the difference between the final results, produced by thermal filter processed and nonfiltered β factor, starts from 0 with no thermal filter applied and asymptotically reaches a constant value.

$$\frac{\partial \beta}{\partial t} = k \frac{\partial^2 \beta}{\partial x^2}, \tag{15}$$

where t is the "time" of the thermal filtering operation.

Since (15) after linearization in the neighborhood of $\beta = 1$ could be represented in terms of (12), the following assumption holds:

$$Q\{B[\Phi(\beta^0, t_f)], t_R\} \approx Q(T^0, t_R + t_f), \tag{16}$$

where t_R is the rifting duration. Hence, if condition

$$Q(T^{(0)}, t_f + t_R) \approx Q(T^0, t_R) \tag{17}$$

is true, then

$$\| Q(T^{(0)}, t_R) - Q(T^{(1)}, t_R) \| \approx 0 \ . \tag{18}$$

This makes the two distributions $T^{(0)}$ and $T^{(1)}$ equivalent, or, in other words, the nonresolvable solutions of the inverse problem.

The thermal filtering operator for (14) was implemented as a simple finite difference method solution of the 1-D diffusion equation. The number N^{Φ} of filter passes required for complete relaxation of the nonresolvable perturbations is

$$N^{\Phi} \approx \frac{1}{\pi} \left(\frac{L}{\Delta x} \right)^2 , \tag{19}$$

where L is the characteristic length scale.

In addition, the Neumann boundary condition of zero lateral heat flow across the vertical model boundaries was adopted. The fulfillment of the condition slightly shifts the integral $\int T(\beta)\,dx$ value of "heat" on each filtering pass. This is corrected by distributing the residual along the cross section on each filtering pass in the shape of $\cos(2x)$. The reason for choosing this function is that it is an eigen-function for (12) and has the slowest exponential decay constant.

Figure 5 illustrates the fulfillment of condition (17). With an increasing number of filtering steps, the difference between the results of the filtered and nonfiltered β profile asymptotically reaches a constant value. The difference is defined as follows:

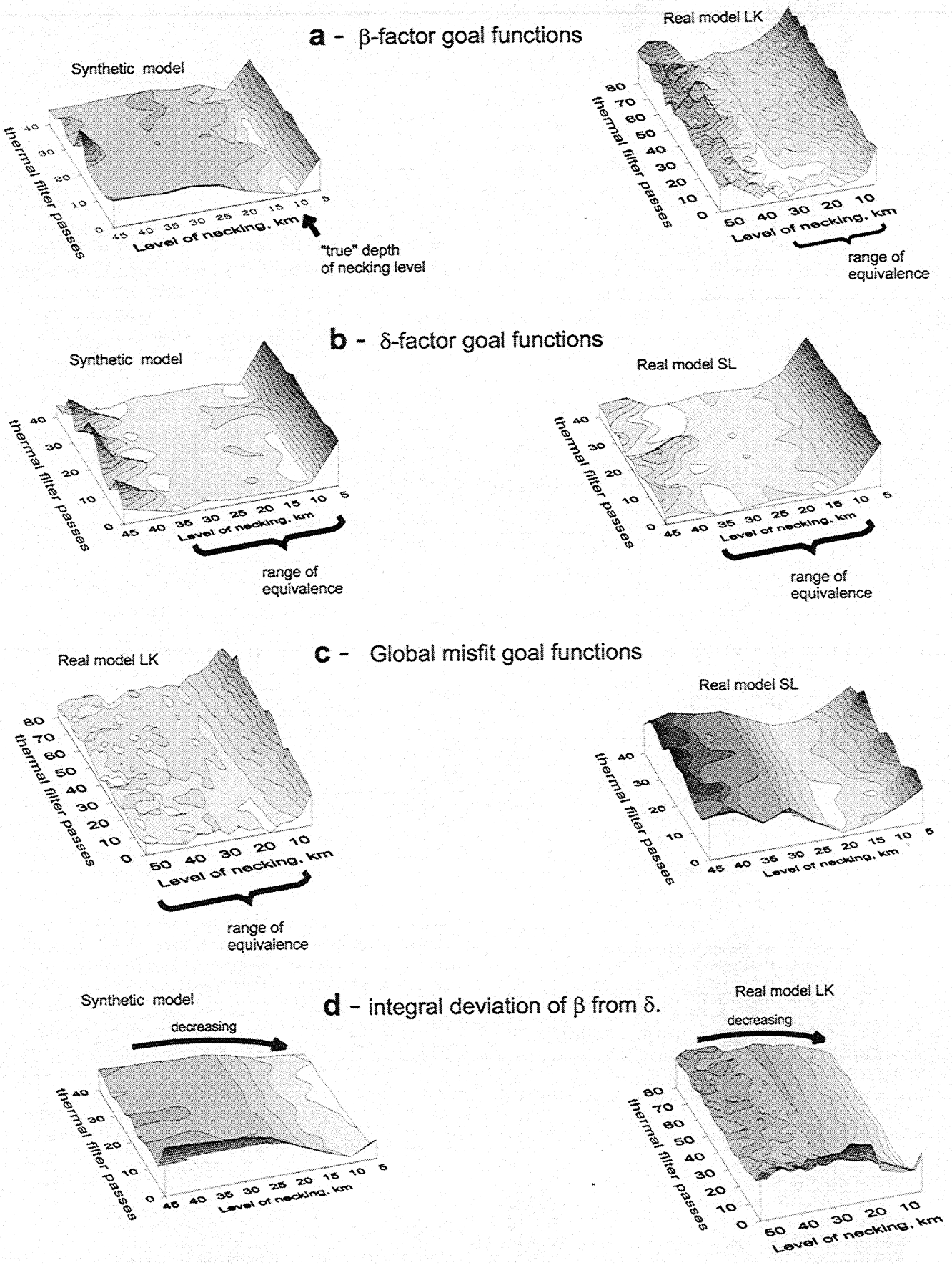

Figure 6. Plots of goal functions (candidates on the role of the necking level goal function) versus necking level and number of thermal filter passes.

$$d^{\beta\beta^0} = \left\| F(X_i) - F\left(X_i^f\right) \right\|, \quad (20)$$

where X_i contains nonfiltered and X_i^f contains filtered β profiles. It is interesting to note that the global misfit value appears to be practically insensitive to the thermal filtering procedure. The β goal function, moreover, decays with an increasing number of filtering steps. This may be seen in Figure 4, where the respective misfit profiles are plotted in addition to filtered and nonfiltered β profiles.

That is to say, the thermal filtering procedure (operator Φ) replaces the initial β factor profile, as it was suggested by the optimizing operator I, by another one, having shape close to the $\cos(2x)$ function. Operator Φ takes care of the integral β factor value conservation and of the boundary condition fulfillment. Both profiles are strictly equivalent for further evolution of the model, as it was shown above. In essence, it means that the optimizing operator I is not capable of resolving individual β values along the profile: it restores integral β value only. This is the limitation of the presented inversion technique.

2.5.2. Optimizing of the level of necking. Many extensional basin forward modeling methods in use incorporate the level of necking parameter, either implicitly [e.g., *Kusznir and Ziegler*, 1992] or explicitly [e.g., *Kooi et al.*, 1992]. The introduction of this parameter can be viewed as a way of combining positive features of two extensional rifting models: the wedge subsidence model of *Vening Meinesz* [1950] and the pure shear/thermal subsidence model of *McKenzie* [1978]. The former predicts rift flank uplift as a result of footwall flexure but fails to explain crust/lithosphere thinning and subsequent basin subsidence. The second model, including its later modifications, cannot explain >500 m uplifted rift shoulders mechanically. It can be argued that these two rather different recent rifting models actually have in common the concept of the lithosphere necking level. However, only the latter (as used in our study) considers this parameter explicitly, which is vitally important in constructing the inverse problem solver.

The depth of lithosphere necking Z_{neck} has a strong influence on the initial subsidence and therefore on the total subsidence value. Hence, Z_{neck} cannot be treated as a second-order parameter and be optimized inside the inner loop of the iterative optimizing operator I. For that reason, we put the optimization of Z_{neck} as an additional outer loop, having operator I inside. This means that operator I optimizes thinning factors only, considering any Z_{neck} value, passed from the outer loop, as a priori known parameter. The outer loop does the Z_{neck} optimization itself. For the Z_{neck} optimization method, we chose regular sampling as the simplest possible technique. Regular sampling can be used here owing to (1) restricted range of Z_{neck} values in X^R ; (2) efficiency of the iterative operator I; and (3) small number of sampling steps (small as far as we may restrict our wish to know the optimal Z_{neck} with high precision). However, some difficulties were encountered with the choice of optimum criteria for Z_{neck}. The set of probable candidates for the role of the Z_{neck} goal function was analyzed during the numerical experiments.

Plots of the β goal function, the δ goal function, the global misfit value, and the integral deviation of β from δ (equation (10)) for the synthetic model and real models are shown in Figure 6 with different necking level values and different thermal filtering step numbers for β. The plot of the β goal function means that the minimum of the β goal function achieved by the operator I was taken as a Z coordinate for the respective point. The X and Y coordinates of this point are the necking level value and the number of thermal filtering steps, respectively.

Figure 6 shows that thermal filtering of the β factor profile does not change significantly the results of operator I for the range of the plotted parameters. Another conclusion that can be made from Figure 6 is that the plotted functions have no profound minimum preserved in all cases.

The β goal function (Figure 6a) strongly points to the "true" value of necking level for the synthetic model but has a wide range of equivalence for the real model LK. The δ goal function (Figure 6b), which intuitively should be the most sensitive parameter (inasmuch as initial subsidence strongly depends on δ factor value), is actually not sensitive for Z_{neck} over a wide range for both synthetic and real models. The statement "not sensitive" here merely means that the iterative operator I is capable of achieving approximately the same minimum of the δ goal function for Z_{neck} in the range ≈10 km to ≈35 km, but the δ factor and/or β factor profiles could differ for different Z_{neck}. The global misfit function (Figure 6c) shows a clear minimum for the real model SL but not for real model LK.

Therefore an additional criterion for Z_{neck} is required, and the minimal integral deviation of β from δ is used. By definition, the deviation of β from δ quantifies the deviation of the current model (suggested, in the present case, by the iterative operator I) from the simplest possible model (i.e., the model with uniform stretching). This parameter almost monotonically decreases with a decrease in Z_{neck} (see Figure 6c). Thus the shallowest necking level (still acceptable in terms of both the global misfit value and the β goal function) is the optimal one.

Hence we assume the linear combination of three goal functions (the β goal function, the global misfit, and the integral deviation of β from δ) as a Z_{neck} goal function $d^{Z_{neck}}$. We define this simply:

$$d^{Z_{neck}} = \frac{1}{N_s} \sum_{m=1}^{N_s} \left(\frac{d_m^{\beta}}{\max d^{\beta}} + \frac{d_m^{G}}{\max d^{G}} + \frac{d_m^{\beta\delta}}{\max d^{\beta\delta}} \right), \quad (21)$$

where $d_m{}^{\beta}$, $d_m{}^{G}$, and $d_m{}^{\beta\delta}$ are the values of the respective goal functions obtained during the regular sampling of the full range of Z_{neck} values, N_s stands for the number of sampling steps, and m is current sampling step number. The minimum of $d^{Z_{neck}}$ then points to an optimal Z_{neck} value. It should be clearly understood that the above mentioned additional criterion of "minimal deviation" has physical meaning of the simplicity of the model. It may be applied in the case of a wide range of equivalence (see Figure 6, real model LK panels) and absence of a priori information about Z_{neck}. With real model SL, there is no need for such an additional criterion inasmuch as the global misfit goal function for this model has the distinct minimum at Z_{neck} = 17 km (see Figure 6c, right).

3. Application

3.1. Dnieper-Donets Basin and Formulation of the Problem

The inverse modeling technique described above has been applied to the Dnieper-Donets Basin (DDB). The DDB is a

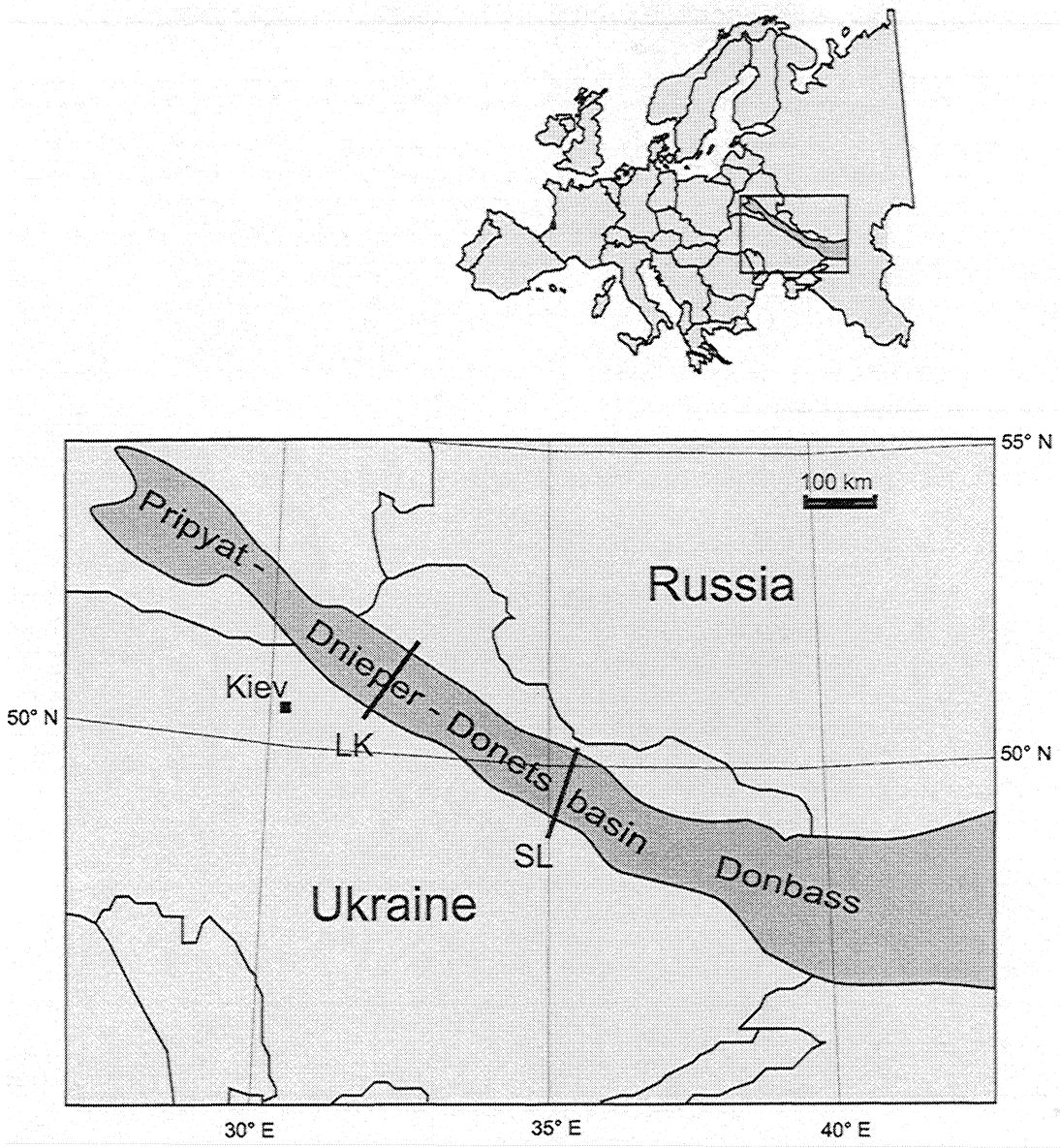

Figure 7. Overview scheme of placement of the Pripyat-Dnieper-Donets-Donbass rift structure and modeled profiles Losinovka-Kinashevka (LK) and Sagajdak-Lebedin (SL) (Figures 8,9).

classical palaeorift structure of the southeastern part of the East European Platform (EEP) (see Figure 7). The basin was formed as a result of intracratonic rifting in the Late Devonian, and it contains up to 19 km of synrift and postrift sediments [e.g., *Stovba et al.*, 1996; *Stovba and Stephenson*, 1999]. The DDB is a central part of a larger rift structure, the Pripyat-Dnieper-Donets-Donbass system, and has a long history of prospecting as one of the oldest oil-gas-bearing provinces of the EEP. The basin has a comprehensive geological-geophysical database, represented by more than 20 regional seismic reflection profiles, a number of regional seismic refraction profiles (including deep seismic sounding), a full set of geophysical field observations, and more than 6000 deep boreholes [cf. *Stovba et al.*, 1996]. Two features of the regional structure of the DDB make it a prospective candidate to test the inversion method: (1) the Carboniferous section is abnormally thick and is difficult to explain by using simple [e.g., *McKenzie*, 1978] models [cf. *van Wees et al.*, 1996; *Kusznir et al.*, 1996; *Starostenko et al.*, 1999] and (2) the intensity of rifting and resulting basin depth increases steadily from northwest to southeast, displaying different intensities of the same process within the frame of a single structure. Salt tectonics affected the postrift sedimentary record of the basin, though this distortion probably is not crucial for modeling purposes, as mass has only been redistributed, rather than removed, from sections.

The tectonic evolution of the DDB has been investigated in detail by a number of geologists. However, only a few attempts at numerical modeling have been undertaken, including 1-D forward and reverse modeling [e.g., *Reverdatto et al.*, 1993; *van Wees et al.*, 1996]. The only 2-D modeling was made by *Kusznir et al.* [1996]. The enlarged Carboniferous thicknesses were explained by *Kusznir et al.*, [1996] by the mantle plume hypothesis. It is expedient, however, to investigate other possible explanations, inasmuch as the thermal doming of the lithosphere may not be consistent with the preservation of the prerift sediments. Prerift sediments have been observed by drilling and seismic

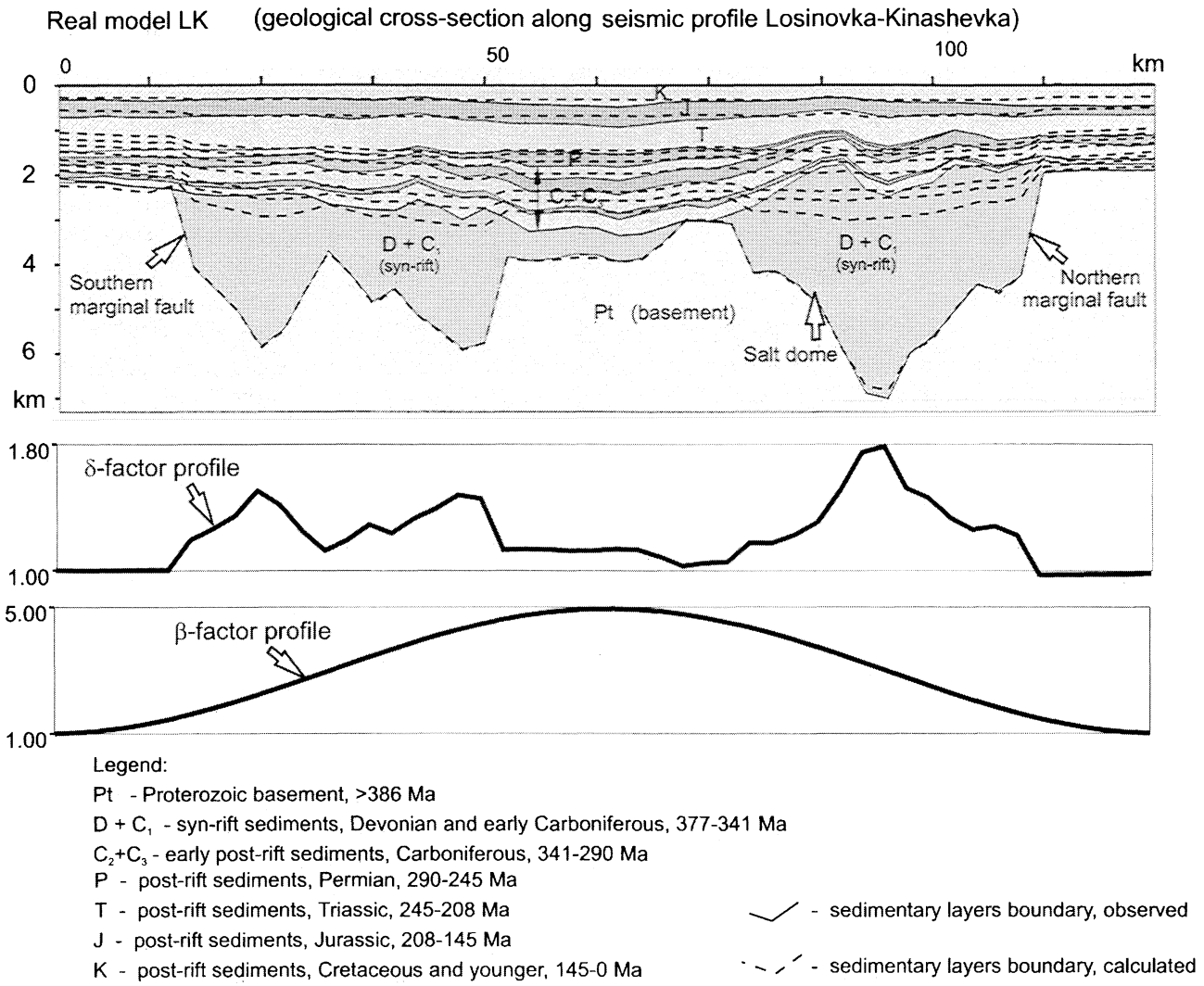

Figure 8. Real model LK (profile Losinovka-Kinashevka, Figure 7). Observed stratigraphy (solid lines) and final model of the calculated stratigraphy (dashed lines). The optimized δ and β profiles for final model are shown at bottom.

reflection data in deep parts of the DDB and in some local grabens on the rift flanks [e.g., *Chirvinskaya and Sollogub*, 1980].

In this study, we assume the generalized tectonic history of the basin, which can be divided into the prominent main synrift phase and a subsequent thermal (postrift) subsidence (see *Stovba et al.* [1996, and references therein] for geological and palaeotectonics details; comprehensive data are also given by *Arsirij et al.* [1984]). The main rifting phase in the DDB started in late Franian time (386 Ma) and lasted up to the end of the Tournesian (350 Ma). Postrift sequences consist of Carboniferous, Permian, Mesozoic, and Paleogene strata, with overall thickness up to 7 km. At least two more rifting phases probably occurred in the basin history, but they were rather weak and cannot be compared (even in cumulative action [cf. *van Wees et al.*, 1996] with the main one in the sense of influence on the postrift evolution. Throughout the whole DDB evolution, the sediments accumulated mostly in a shallow marine environment (the water depth does not exceed 100 m in the area studied), so we may neglect the palaeobathymetric changes.

We modeled two regional seismic profiles (N.K.Kivshik et al., preprint, The Regional Seismostratigraphic Prospects in the Dnieper-Donets Depression, 1993). The first, Losinovka-Kinashevka (LK), is situated in the northwest (shallower) part of the basin, and the second one, Sagajdak-Lebedin (SL), is in the central part of the basin (see Figure 7). Both profiles cross the DDB from flank to flank. The full set of the inverse problem solver algorithms and some special additions (see below) were applied to both profiles.

Overall, our purpose was to test our methodology on a real basin. A special focus in the present case is the abnormally thick Carboniferous section and whether it could be explained in terms of the variations of parameters. The forward problem solver parameter set (nonhomogeneous thinning factors, variable flexural rigidity of the lithosphere, intraplate stress-induced variations in subsidence during the postrift evolution of the basin, etc.) did not include the additional tectonic event (intrinsic to the DDB) hypotheses.

3.2. Results and Geological Implications for the DDB

3.2.1. Calculated and Observed Stratigraphy. Figures 8 and 9 illustrate observed (solid lines) and calculated (dashed lines) stratigraphic crosssections for LK and SL profiles, respectively. The greatest discrepancies between the observed

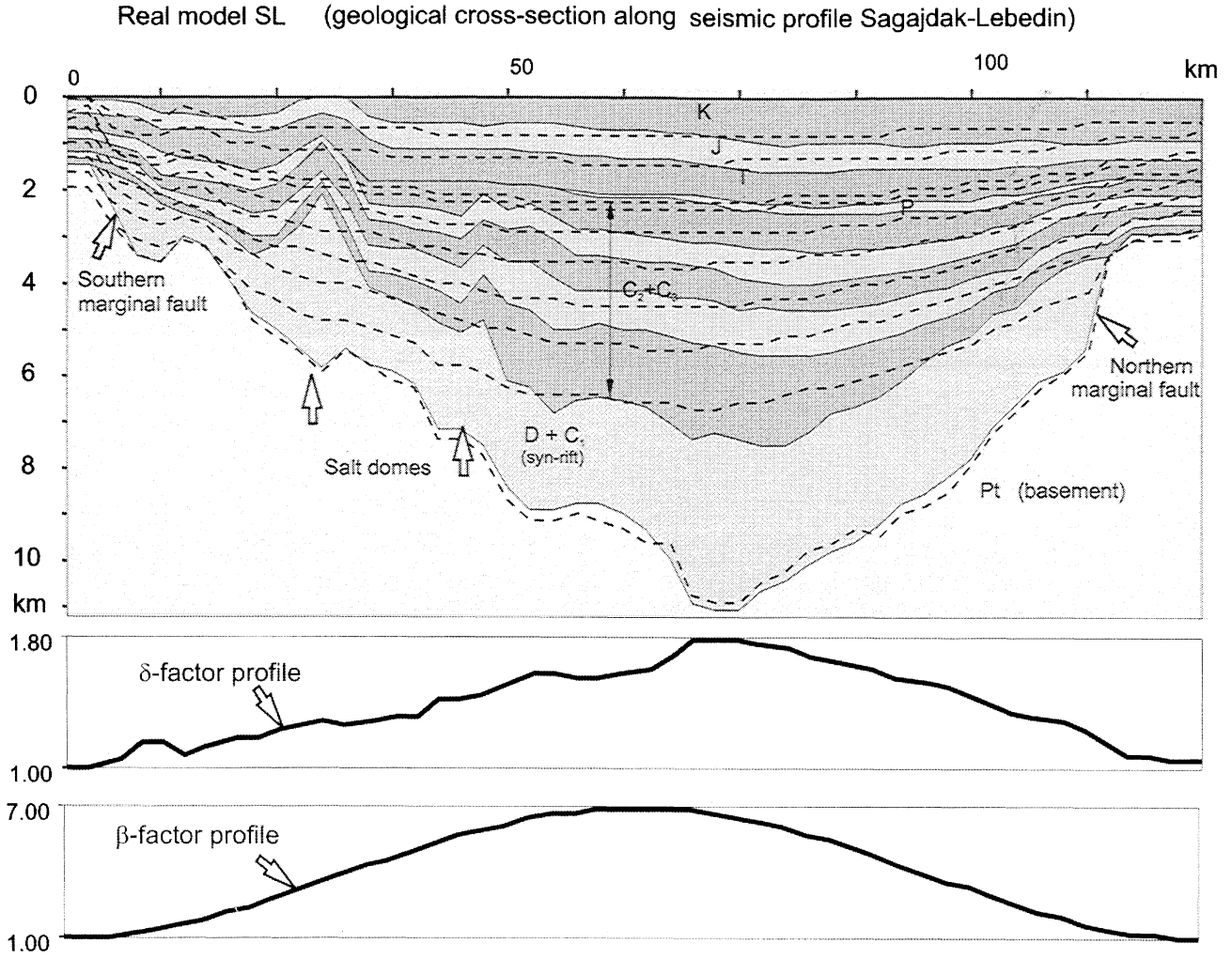

Figure 9. Real model SL (profile Sagajdak-Lebedin, Figure 7). Observed stratigraphy (solid lines) and final model of the calculated stratigraphy (dashed lines). The optimized δ and β profiles for the final model are shown at bottom.

and calculated horizon depths occur in the deepest part (central graben) of the basin. Although the inverse problem algorithm is focused on the coincidence of the averaged layer thicknesses rather than on horizon depths, the observed discrepancies are not an artifact of the method. This misfit could not be satisfied by varying any parameter from vector X (this was verified by a series of numerical experiments). Rather, it is inferred that the sediment accumulation was disturbed by salt tectonics. Salt domes are situated fairly close to the profiles modeled (see Figures 8 and 9), in both cases adjacent to the places of greatest discrepancies, where short wavelength relief is seen in postrift strata. There is, however, strong evidence [cf. *Chirvinskaya and Sollogub*, 1980; *Arsirij et al.*, 1984] for rather linear shapes of main salt bodies, oriented along the marginal faults. This leads us to the conclusion that the sediment redistribution did not massively violate the two dimensionality and is not therefore crucial for modeling purposes.

In general, the inverse modeling results in a good coincidence of calculated and observed basement depths (i.e., the sum of all thicknesses), with a satisfactory fit within the section in respect of depth and thickness for any individual horizon. Note that the calculations involve flexural and heat conduction effects, both in 2-D.

3.2.2. Thinning factors. Optimized δ and β factor profiles are plotted at the bottom of Figures 8 and 9. Note that the SL cross section with the greatest thickness of sediments does not require a higher maximum δ factor than the LK profile, although the average value of δ factor for SL is higher than that for LK (1.39 and 1.23, respectively). The subcrustal thinning factor β, in contrast, has a much higher maximum on SL than on LK (7 versus 5). Averaged β factor values are 2.97 for the LK profile and 3.95 for the SL profile. The ratio of distances between the marginal faults for the two cross sections agrees well with the ratio of the averaged δ factor values (1.14 and 1.13, respectively). This agreement confirms the validity of the initial crustal lithosphere parameters adopted and argues in favor of the single rifting phase approximation. The regular increase of the averaged crustal thinning factors from the LK profile to the SL profile also confirms the qualitatively formulated geological hypothesis of *Chekunov* [1994] concerning the scissors-like style of the DDB opening during the main rifting phase.

Maximal (and even average) β factor values obtained for both profiles are considerably higher than those which are usually considered as typical for syn rift volcanic activity [*Wilson*, 1989]. These high β factor values were required by the inverse problem solver in order to explain the enlarged thicknesses of the Carboniferous sediments being accumulated in the DDB immediately after the end of the main rifting phase. A high β factor value (considerably higher than the δ factor value) is a numerical equivalent of the additional amount of heat being introduced into the model. Therefore the results obtained are similar to those of *Kusznir et al.* [1996]. This means that the contradiction remains between the "additional plume hypothesis" and the presence of the pre rift sediments in the DDB. However, the β factor value should be considered as an effective (cumulative) parameter, as will be discussed in section 4. Numerical evaluation of the phase transition effect [see, e.g., *Podladchikov et al.*, 1994, and references therein] will significantly decrease the required β factor values and in this way will help to overcome the contradiction.

3.2.3. Level of lithosphere necking. According to the Z_{neck} goal function choice and the method of its minimization described above, the inverse problem solver suggested depths of lithosphere necking of 10 km and 17 km for the LK profile and the SL profile, respectively, and these values were used in subsequent calculations. Values are relatively small and allow us to include both profiles in the group of models with so-called shallow necking level. However, the inferred shallow level of lithospheric necking implies little or no rift flank uplift, which contrasts with some geological evidence suggesting considerable erosion of the rift shoulders [cf. *Chirvinskaya and Sollogub*, 1980; *Stovba et al.*, 1996]. At present, there is no reliable estimate of the degree of erosion (although *Kusznir et al.* [1996] made indirect estimates on the basis of forward and reverse modeling results), and all that can be said further is that some degree of rift flank erosion does not in itself contradict the present model results but that a large amount of erosion does. New estimations of the magnitude of erosion should be available soon when the results of the fission-track analyses of samples from the basin flanks basement are published, allowing us to evaluate the "shallow level of necking" prediction.

4. Discussion and Conclusions

Using terms from communication theory, vector X in (2) is the initial message, encoded by the encoding algorithm F_{true} (the "true" response function of the lithosphere), and the observed stratigraphy $Y_{observed}$ is the encoded message obtained. Our purpose is to decode the message $Y_{observed}$ in order to restore the initial message X. According to the basic principles of communication theory [e.g., *Shannon*, 1959], in order to correctly decode the message received one must know the true encoding algorithm F_{true}. Doing modeling of the rift evolution, we are dealing, however, with the encoding algorithm (or forward problem operator) F, which is only an approximate representation of the true response function of the lithosphere F_{true}. This means that F_{true} necessarily contains some natural processes which are not taken into account by its mathematical approximation, operator F. Let us call the processes included in operator F "disclosed" in contrast to "cryptic" [cf. *Slingerland et al.*, 1994] processes, assuming that cryptic processes are part of F_{true} but are not included yet in the operator F.

The effects of cryptic processes will definitely appear in the observed stratigraphy $Y_{observed}$ inasmuch as $Y_{observed}$ is a function of F_{true} rather than a function of F. Any modeling technique, by definition, is dealing with the approximation F. This results in "smearing", to borrow the terminology used in seismic tomography. In practice, this means that any modeling will inevitably place the effect of a cryptic process inside the effect of a disclosed process and therefore will distort the actual picture. In fact, this happens with β factor values. The β factor becomes the first victim of smearing for the simple reason that this parameter is more poorly constrained by the data than others.

Probably the most significant of the cryptic processes is the isostatic effect of the phase transition, occurring in the lower lithosphere and upper mantle because of rifting (as shown by *Podladchikov et al.* [1994]). Phase transitions work in the same direction as an increase in β factor values. This leads to the conclusion that the β factor profile as it is restored by the modeling should be interpreted as an effective (cumulative) parameter. In other words, a β factor of 7 does not literally mean that the mantle layer of lithosphere has been thinned by a factor of 7 during the rifting.

An accurate estimate of the β factor is especially important while doing rifting modeling for the prediction of oil and gas maturation potential of an observed basin. In this case, evaluation of the heat input (the β factor values) is crucial; hence the phase transition effect should be quantitatively estimated and taken into account. The inverse modeling technique opens the way for further development in this direction, allowing incorporation of new (currently cryptic) natural processes into the forward problem solver. This possibility arises because of the dramatically decreased number of parameters that need to be adjusted manually by the interpreter.

Acknowledgments. We acknowledge the indispensable help of specialists from Ukrgeofizika (Kiev, Ukraine) who provided the interpretation of seismic reflection and well data and built the geological cross sections used in this work, in particular S. Stovba for geological consultations concerning the sedimentary cover of the Dnieper-Donets Basin. We also acknowledge V. Starostenko (IGF NANU, Kiev, Ukraine) for his guidance regarding inverse problems theory and N. Kusznir (University of Liverpool, Liverpool, UK) for his always generous advice regarding aspects of 2-D forward modeling of sedimentary basins. We thank S. A. Hall (University of Houston, U.S.A.) for his valuable recommendations with discussion and conclusions. We acknowledge with thanks the help of Associate Editor C. Ebinger and referees N. White, J. Stewart and M.A. Menzies. The work leading to this paper was carried out in the framework of EUROPROBE, a program of the European Science Foundation, with funding from INTAS project 93-3346 and EUROPROBE. This is a Netherlands Research School of Sedimentary Geology contribution.

References

Arsirij, Y.A., V.A.Vitenko, A.M. Palij, and A.K. Tsypko (Eds.), *Atlas of the Geological Structure and the Oil-Gas Bearingness of the Dnieper-Donets Depression* (in Russian), 190 pp., Kiev, Ukrainian Geol. Comm., 1984.

Braun, J., and C. Beaumont, A physical explanation for the relationship between flank uplifts and the breakup unconformity at rifted continental margins, *Geology*, *17*, 760-764, 1989.

Chekunov, A.V., On the hinge joint of the Pripyat and Dniepr grabens (in Russian), *Dopov. Akad. Nauk Ukr.*, *3*, 101-105, 1994.

Chirvinskaya, M.V., and V.B. Sollogub, *Deep Structure of the Dnieper-Donets Aulakogen From Geophysical Data* (in Russian), 177 pp., Nauk. Dumka, Kiev, 1980.

Cloetingh, S. and H. Kooi, Intraplate stresses and dynamical aspects of rift basins, *Tectonophysics*, *215*, 167-185, 1992.

Cloetingh, S., H. McQueen, and K. Lambeck, On a tectonic mechanism for regional sea level variations, *Earth Planet. Sci. Lett.*, *75*, 157-166, 1985.

Jarvis, G.T., and D.P. McKenzie, Sedimentary basin formation with finite extension rates, *Earth Planet. Sci. Lett.*, *48*, 42-52, 1980.

Karner, G.D., Effects of lithospheric in-plane stress on sedimentary basin stratigraphy, *Tectonics*, *5*, 573-588, 1986.

Kooi, H., and S. Cloetingh, Lithospheric necking and regional isostasy at extensional basins, 2, Stress induced vertical motions and relative sea level changes, *J. Geophys. Res.*, *97*, 17,573-17,591, 1992.

Kooi, H., S. Cloetingh, and J. Burrus, Lithospheric necking and regional isostasy at extensional basins, 1, Subsidence and gravity modeling with an application to the Gulf of Lions Margin (SE France), *J. Geophys. Res.*, *97*, 17,553-17,571, 1992.

Kusznir, N.J., P.A. and Ziegler, The mechanics of continental extension and sedimentary basin formation: A simple-shear/pure-shear flexural cantilever model, *Tectonophysics*, *215*, 117-131, 1992.

Kusznir, N.J., S.M. Stovba, R.A. Stephenson, and K.N. Poplavskii, The formation of the northwestern Dniepr-Donets Basin: 2D forward and reverse syn-rift and post-rift modelling, in *EUROPROBE: Intraplate Tectonics and Basin Dynamics of the Eastern European Platform,* edited by R.A. Stephenson et al., *Tectonophysics*, *268*, 237-255, 1996.

McKenzie, D.P., Some remarks on the development of sedimentary basins, *Earth Planet. Sci. Lett.*, *40*, 25-31, 1978.

Menke, W., Geophysical Data Analysis: Discrete Inverse Theory, 260 pp., Academic, San Diego, Calif., 1984.

Podladchikov, Yu.Yu., Poliakov, A.N.B., Yuen D.A., The effect of lithospheric phase transitions on subsidence of extending continental lithosphere, *Earth Planet. Sci. Lett.*, 124, 95-103, 1994.

Reverdatto, V.V., O.P. Polyansky, and A.V. Chekunov, The evolution of Dnieper-Donets aulacogen in comparison with north-European rifts (in Russian), *Dokl. Ross. Akad. Nauk*, *330* (5), 620-623, 1993.

Royden, L. and C.E. Keen, Rifting process and thermal evolution of the continental margin of eastern Canada determined from subsidence curves, *Earth Planet. Sci. Lett.*, *51*, 343-361, 1980.

Shannon, C.E., *The Mathematical Theory of Communication*, 117 pp., Univ. of Ill. Press, Urbana, 1959.

Slingerland, R., J.W. Harbaugh, and K. Furlong, *Simulating Clastic Sedimentary Basins: Physical Fundamentals and Computer Programs for Creating Dynamic Systems*, Sediment. Geol. Ser., 220 pp., Prentice-Hall, Englewood Cliffs, N. J., 1994.

Starostenko, V.I., V.A. Danilenko, D.B. Vengrovitch, and K.N. Poplavskii, A fully dynamic model of continental rifting applied to the syn-rift evolution of sedimentary basins, in *EUROPROBE: Intraplate Tectonics and Basin Dynamics of the Eastern European Platform,* edited by R.A. Stephenson et al., *Tectonophysics*, *268*, 237-255, 1996.

Starostenko, V.I., V.A. Danilenko, D.B. Vengrovitch, R.I. Kutas, S.M. Stovba, R.A. Stephenson, and O.M. Kharitonov, A new geodynamical-thermal model of rift evolution, with application to the Dnieper-Donets Basin, Ukraine, in *EUROPROBE Georift, volume 2 : Intraplate Tectonics and Basin Dynamics on the Eastern European Craton and its Margins,* edited by R.A. Stephenson, M. Wilson, and V.I. Starostenko, *Tectonophysics*, *313*(1-2), 29-40, 1999.

Stephenson, R., and K. Lambeck, Isostatic response of the lithosphere with in-plane stress: Application to central Australia, *J. Geophys. Res.*, *90*, 8581-8588, 1985.

Stephenson, R., S.M. Nakiboglu, and M.A. Kelly, Effects of asthenosphere melting, regional thermoisostasy and sediment loading on the thermomechanical evolution of extensional sedimentary basins. In: *Origin and Evolution of Sedimentary Basins and Their Energy and Mineral Resources, Geophys. Monogr. Ser.,* vol.48, edited by R.A. Price, pp. 17-27, AGU, Washington, D.C., 1989.

Stovba, S.M, and R.A. Stephenson, The Donbas Foldbelt: its relationships with the uninverted Donets segment of the Dniepr-Donets basin, Ukraine, in *EUROPROBE Georift, volume 2 : Intraplate Tectonics and Basin Dynamics on the Eastern European Craton and its Margins,* edited by R.A. Stephenson, M. Wilson, and V.I. Starostenko, *Tectonophysics*, *313*(1-2), 59-83, 1999.

Stovba, S.M, R.A. Stephenson, and M. Kivshik, Structural features and evolution of the Dnieper-Donets basin, Ukraine, from regional seismic reflection profiles, in *EUROPROBE: Intraplate Tectonics and Basin Dynamics of the Eastern European Platform,* edited by R.A. Stephenson et al., *Tectonophysics*, *268*, 237-255, 1996.

van Wees, J.D., R.A. Stephenson, S.M. Stovba, and V.A. Shymanovskyi, Tectonic variation in the Dnieper-Donets basin from automated modelling of backstripped subsidence curves, in *EUROPROBE: Intraplate Tectonics and Basin Dynamics of the Eastern European Platform,* edited by R.A. Stephenson et al., *Tectonophysics*, *268*, 237-255, 1996.

Vening Meinesz, F.A., Les graben africains, résultat de compression ou de tension dans la croûte terrestre?, *Inst. R. Colon. Belge Bull. Seances*, *21*, 539-552, 1950.

Watts, A.B., and J. Stewart, Gravity anomalies and the segmentation of the continental margin offshore West Africa, *Earth Planet. Sci. Lett.*, *156*, 239-252, 1998.

White, N., Recovery of strain rate variation from inversion of subsidence data, *Nature*, *366*, 449-452, 1993.

White, N., An inverse method for determining lithospheric strain rate variation on geological timescales, *Earth Planet. Sci. Lett.*, *122*(3-4), 351-371, 1994.

Wilson, M., *Igneous Petrogenesis: A Global Tectonic Approach*, 466 pp., Unwin Hyman, Boston, Mass., 1989.

Y.Y. Podladchikov, Geologisches Institut, ETH-Zurich, Zurich, Switzerland. (yura@erdw.ethz.ch)

K.N. Poplavskii, Geosciences Department, University of Houston, 4800 Calhoun Road, SR-1 Room 312, Houston, TX, 77204-5503. (kpoplavs@uh.edu)

R.A. Stephenson, Department of Sedimentary Geology, Vrije Universiteit, Amsterdam, Netherlands. (ster@geo.vu.nl)

(Received December 30, 1997; revised April 19, 1999;
accepted June 11, 1999.)